Variable antennas positions solution to reduce pointing errors due to wind speed and temperature coupled effects during free space optical link using matrix Rician pointing error model

Michel TEUMA MBEZI*, Samuel EKE, Idelette Hermine Judith SOM, Ruben Martin MOUANGUE

National Higher Polytechnic School of Douala, University of Douala, P.O. Box 2701, Douala, Cameroon

*Corresponding author: 3michelteuma@gmail.com

Pointing errors (PE) during free space optical (FSO) transmission can be caused by laser beam wander due to thermal and wind dynamic instability. The aim of this work is to study the coupled effects of temperature and wind speed on PE using matrix Rician pointing error (MRPE) model; then show how variable antennas height can reduce PE due to wind speed and temperature coupled effects. To achieve this purposes, average PE expression was established using MRPE model. Then considering a Gaussian beam wave and Monin–Obukhov similarity functions for the structure parameters of temperature, explicit relationship was established between average PE, temperature and wind speed. It comes out of this study that under dynamic turbulence, one can appropriately modify temperature to reduce PE due to dynamic instability and reciprocally. Depending on turbulence large cells or frozen turbulence eddies distribution, PE can be reduced by appropriately modified antennas height or the distance between transmitter and receiver. That is why this work suggests to install variable or dynamic antennas (rather than fixed ones) which could intelligently modify its positions according to *laser beam wander* created by atmospheric turbulence.

Keywords: atmospheric turbulence, pointing errors, free space optical transmission, Rician pointing error model.

1. Introduction

With comparable high speed as optical fiber (over 10 Gbps) [1], free space optical (FSO) transmission is flexible due to its wireless transmission and allows all data types transmission. In addition to the fact that its production cost is lower than that required for the deployment of optical fiber (its license-free bandwidth) [2-9], its implementation and maintenance in the field is less restrictive. However, because FSO signals are propagated through the air, some environmental challenges are unavoidable. Thus, before arriving at the receiver, laser beams are principally affected by atmospheric turbulence, path losses, and pointing errors (PE) respectively represented by h_a, h_l and

h_p coefficients; so that the channel state or instantaneous intensity gain can be expressed as

$$h = h_a h_l h_p \tag{1}$$

In fact, atmospheric turbulence is due to thermal instability and wind dynamic instability; these thermal and wind dynamic instabilities lead to a fluctuation of air cells and cause random eddies of different sizes. Depending of eddies scale sizes, if the size of the turbulence eddies is larger than the laser beam diameter, the whole laser beam bends, as shown in Fig. 1 (*beam wander*). However, we observed *beam scintillation*, if the size of the eddies is smaller than the optical beam size.
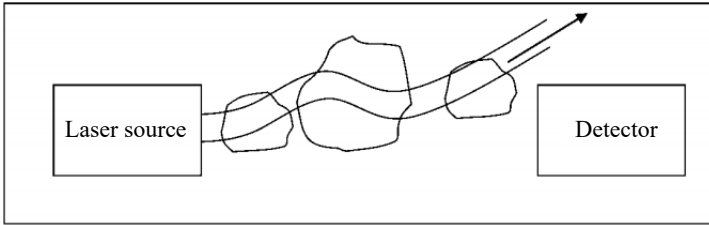

Fig. 1. Laser beam wandering due to turbulence cells that are larger than the beam diameter [11].

Misalignment or PE can occur due to a variety of reasons, such as swinging of buildings, earthquakes, and heavy wind [10]. In addition to the above classical causes of PE, we can observe in Fig. 1 that beam wandering can be related to PE since the emitted signal is not received by the receiver in spite of the fact that the transmitter and receiver are aligned and that the emitted signal could be received by the receiver of slight changed position. In addition, PE can be due to the presence of frozen eddies in the line-of-sight (LOS) of the transmitter and receiver as showed in Fig. 2. So, by simultaneous modify of positions of the transmitter and receiver we can avoid the frozen eddies to be between the LOS.
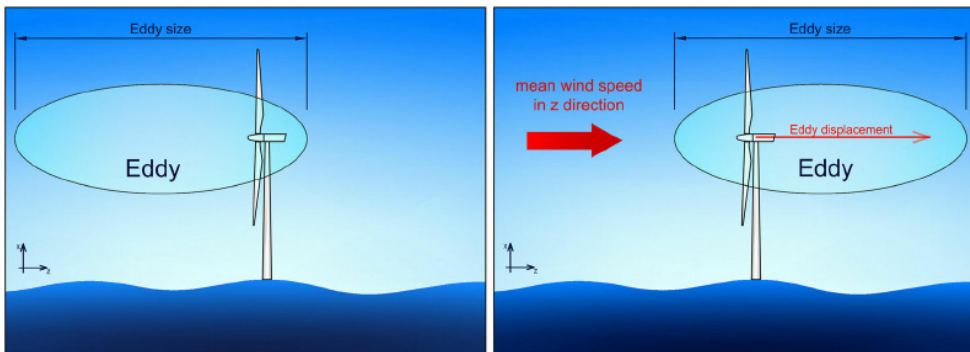

Fig. 2. Taylor's frozen turbulence hypothesis: an eddy travels with the mean wind speed, while its size and characteristic parameters remain constant [12].

Many studies have been made to show how pointing error affect FSO transmission by establishing relations between bit error rate, outage probability, capacity and PE [13-28]. In the article published in [27], ANSARI *et al.*, analyze the performance of free-space optical links with pointing errors. In [28], ALSHAER *et al.*, used a non-zero-boresight pointing error to make a generic evaluation of FSO system over Málaga turbulence channel. More recently, in 2022 HAN *et al.*, studied the joint impact of channel estimation error and pointing error on FSO communication systems [25]. The same year (2022) DING *et al.* studied the dual-hop RF/FSO systems with non-zero boresight pointing errors [24]. In general, these cited research works and many others [29-33] investigated how pointing error affected FSO transmission; but so far, according to our knowledge, temperature and wind speed coupled effects on PE have not yet been investigated. That is why the first purpose of this work is to study the coupled effects of temperature and wind speed on PE during FSO transmission using a new formulation of Rician pointing error (RPE) model, namely matrix Rician pointing error (MRPE) model. Then we show that using a variable antennas positions could lead to reduction of PE. The rest of the paper is therefore presented as follows: In Section 2, we have explained methods used to obtain results which are presented and discussed in Section 3. Section 4 is devoted to some concluded remarks of the paper.

2. Methods

Knowing that the current form of Rician pointing error model is not appropriate to achieve the purposes of this work since it is defined as a function (PDF), the matrix Rician pointing error (MRPE) model is going to be defined as a matrix probability density function. After, average PE is going to be expressed using the MRPE model. In this study, we consider a Gaussian beam that propagates along the z axis.

2.1. Matrix Rician pointing error model

Based on RPE model [34], we defined the matrix elements $f^{pq}(h_{\mathrm{p}}^{pq})$ of the matrix probability density function of MRPE $f(h_{\mathrm{p}})$ which induced PE factors matrix h_{p}, (with matrix elements h_{p}^{pq}) as

$$f^{pq}(h_{\mathrm{p}}^{pq}) = \frac{\xi_{pq}^2}{(A_0^{pq})^{\xi_{pq}^2}} \exp\left(\frac{-s_{pq}^2}{2\sigma_{pq}^2}\right) I_0\left(\frac{s_{pq}}{\sqrt{2}\, s_{pq}^2} \sqrt{-w_{zeq}^{pq}\ln\left(\frac{h_p^{pq}}{A_0^{pq}}\right)}\right),$$

$$0 \le h_{\mathrm{p}}^{pq} \le A_0^{pq} \tag{2}$$

where σ_{pq} is the PE displacement standard deviation matrix element at the receiver, σ_{pq}^2 is the jitter variance matrix element at the receiver. The boresight displacement matrix element s_{pq} is assumed to be expressed as

$$s_{pq} \cong \frac{1}{2}(w_z^{pq} - w_0 \pm \sigma_{pq}) \tag{3}$$

where w_z^{pq} is the beam width at z distance from the transmitter; w_0 is the beam spot radius at the transmitter ($z = 0$); it is defined as [28]

$$w_0 \cong \frac{\lambda}{\pi \alpha} \tag{4}$$

where λ is the light wavelength and α is the half of divergence angle. Equivalent beam width matrix element w_{zeq}^{pq} is related to the maximum fraction of the collected power matrix element (at $r = 0$), A_0^{pq} is the amount of ratio between aperture radius of receiver a with the beam width w_z^{pq} matrix element v_{pq}; the wave number k; the distance between the transmitter and the receiver L, and the refractive index structure parameter matrix element C_n^{pq} through the following relations [28,34]:

$$w_{zeq}^{pq} = (w_z^{pq})^2 \frac{\sqrt{A_0^{pq} \pi}}{2 v_{pq} \exp(-v_{pq}^2)} \tag{5}$$

$$v_{pq} = \sqrt{\frac{\pi a^2}{2 w_z^{pq}}} \tag{6}$$

$$w_z^{pq} = w_0 \sqrt{1 + \varepsilon_{pq} \left(\frac{\lambda L}{\pi w_0^2} \right)} \tag{7}$$

$$\varepsilon_{pq} = 1 + \frac{2 w_0^2}{(\rho_0^{pq})^2} \tag{8}$$

$$\rho_0^{pq} = \left[0.55 (C_n^{pq})^2 k^2 L \right]^{-3/5} \tag{9}$$

$$A_0^{pq} = \left[\mathrm{erf}(v_{pq}) \right]^2 \tag{10}$$

and $I_0(\cdot)$ is the modified Bessel function of the first kind with 0 order.

$$\xi_{pq} = \frac{w_{zeq}^{pq}}{2 \sigma_{pq}} \tag{11}$$

represents the quantitative relation between the equivalent beam width and the jitter variance.

2.2. Average pointing error

Base on the PDF of Beckmann distribution express in [35,36], the n-th moment of h_p derived on [34], we deduced the average matrix element PE $\overline{h_p^{pq}}$ by using MRPE as follows:

$$\overline{h_{\mathrm{p}}^{pq}} \; = \; \frac{A_0^{pq} \, \xi_{pq}^2}{1 + \xi_{pq}^2} \; \exp\left(- \frac{2 \, \xi_{pq}^2 \, s_{pq}^2}{(w_{zeq}^{pq})^2 \, (1 + \xi_{pq}^2)} \right) \tag{12}$$

The above equation is related to temperature and wind speed though the refractive index structure parameter matrix element $(C_n^{pq})^2$. Knowing that PE due to laser beam wander is related to large scale atmospheric turbulence, the jitter can be assumed to be the variance of large-scale atmospheric turbulence [10] such that, we can write:

$$\sigma_{pq}^2 \; = \; (\sigma_x^{pq})^2 \; = \; \exp\left[(\sigma_{lnx}^{pq})^2 \right] - 1 \tag{13}$$

2.3. $(C_n^{pq})^2$ and $(\sigma_{lnx}^{pq})^2$ expressions

To describe beam at a given position $z = L$, the following parameters (input-plane beam parameters, and output plane beam parameters corresponding to the input-plane beam parameters) are usually used [10, 37-39]: the curvature parameter θ_0, the Fresnel ratio at the input plane Λ_0, the radius of curvature F_0 which specifies the beam forming, the radius of curvature at the receiver F, the beam spot radius at the receiver W, the Fresnel ratio characterizing the radius of Gaussian lens Ω_G. Relations between the above parameters are given as follows:

$$\begin{cases} \theta_0 \; = \; 1 - \dfrac{L}{F_0} \\[2mm] \Lambda_0 \; = \; \dfrac{2L}{kW_0} \\[2mm] \Lambda \; = \; \dfrac{\Lambda_0}{\theta_0^2 + \Lambda_0^2} \; = \; \dfrac{2L}{kW} \end{cases} \tag{14}$$

$$\begin{cases} W \; = \; W_0(\theta_0^2 + \Lambda_0^2)^{1/2} \\[2mm] W_0 \; \cong \; \dfrac{\lambda}{\pi \alpha} \end{cases} \tag{15}$$

$$\begin{cases} \overline{\theta} \; = \; 1 - \theta \\[2mm] \theta \; = \; \dfrac{\theta_0}{\theta_0^2 + \Lambda_0^2} \; = \; 1 - \dfrac{L}{F} \\[2mm] \Omega_G \; = \; \dfrac{16L}{kD^2} \end{cases} \tag{16}$$

where θ is the output-plane beam parameter corresponding to the input-plan beam parameter θ_0, D is the diameter of the receiver lens. $(\sigma_{lnx}^{pq})^2$ matrix element is expressed as

$$(\sigma_{lnx}^{pq})^2(D, L) = 0.49(\sigma_1^{pq})^2 \left(\frac{\Omega_G - \Lambda}{\Omega_G + \Lambda}\right)^2 \left(\frac{1}{3} - \frac{1}{2}\overline{\theta} + \frac{1}{5}\overline{\theta}^2\right)$$

$$\times \frac{(\eta_x^{pq})^{7/6}}{\left(1 + 0.40\, \eta_x^{pq}\, \dfrac{2 - \overline{\theta}}{\Omega_G + \Lambda}\right)^{7/6}} \tag{17}$$

where η_x^{pq} is artificial matrix elements variable defined as

$$\eta_x^{pq} = \frac{1}{1 + 0.56(\sigma_B^{pq})^{12/5}} \left(\frac{1}{3} - \frac{1}{2}\overline{\theta} + \frac{1}{5}\overline{\theta}^2\right)^{-6/7} \left[\frac{(\sigma_B^{pq})^2}{(\sigma_1^{pq})^2}\right]^{6/7} \tag{18}$$

Matrix elements $(\sigma_B^{pq})^2$, $(\sigma_1^{pq})^2$ are Rytov variance for Gaussian-beam wave and plane wave, respectively. They are expressed as

$$\begin{cases} (\sigma_B^{pq})^2 = 3.86(\sigma_1^{pq})^2 \left\{\frac{2}{5}\left[(1 + 2\theta)^2 + 4\Lambda^2\right]^{\frac{5}{12}} \cos\left[\frac{5}{6}\tan^{-1}\left(\frac{1 + 2\theta}{2\Lambda}\right)\right] - \frac{11}{6}\Lambda^{\frac{5}{6}}\right\} \\[2em] (\sigma_1^{pq})^2 = 1.23(C_n^{pq})^2\, k^{\frac{7}{6}}\, L^{\frac{11}{6}} \end{cases} \tag{19}$$

where $(C_n^{pq})^2$ is the refractive-index structure matrix parameter element. The relationship between refractive-index structure and temperature structure C_T^2 provided by [40] is expressed in Eq. (20). $P(h)$ is pressured at altitude h expressed in Eq. (21) (international barometric leveling formula). $T(h)$ is temperature at altitude h expressed in Eq. (21) using Reynold decomposition where $\overline{T}(h)$ is the Reynold mean and $T'(h)$ the temperature fluctuation at h altitude.

Experimental study was made by [41] using Monin–Obukhov similarity functions for the structure parameters of temperature, to provide an analytical expression which relates temperature structure C_T^2 to some characteristic atmospheric parameters. That analytical expression for unstable atmospheric conditions is as follows:

$$\begin{cases} (C_n^{pq})^2 = \left[79 \times 10^{-6}\, \frac{P(h)}{T(h)}\right]^2 C_T^2 \\[2em] C_T^2 = \dfrac{T_*^2}{(k_0 h)^{\frac{2}{3}}}\, C_{T1}\, k_0^{\frac{2}{3}} \left(1 - C_{T2}\, \frac{h}{L_0}\right)^{-\frac{2}{3}} \end{cases} \tag{20}$$

where C_{T1} and C_{T2} are constants which were determined experimentally, k_0 is the Von Karman constant, h is the measurement height. T_*, L_0, u_*, are surface-layer temperature scales, Obukhov length scale, friction velocity, respectively, and are defined in Eqs. (21) and (22). The prime denotes the turbulent fluctuations, while the overbar denotes the Reynolds average, u, and w denote the stream wise and vertical velocities, respectively.

$$
\begin{cases}
P(h) &= 1013.25 \left(1 - \dfrac{0.0065h}{288.15} \right)^{5.255} \\[2mm]
T(h) &= \overline{T}(h) + T'(h) \\[2mm]
T_* &= -\dfrac{H}{\rho_{\text{air}} C_{\text{p}} u_*}
\end{cases}
\tag{21}
$$

where H is the surface sensible heat fluxes (W m^{-2}), ρ_{air} is the air density, g is the gravitational acceleration, q is the specific humidity, C_{p} is the air specific heat capacity at constant pressure [42] given by

$$
\begin{cases}
L_0 &= \dfrac{\overline{T} u_*^3}{k_0 g(\overline{w'T'} + 0.61 \overline{\overline{T} w'q'})} \\[4mm]
u_* &= k_{\text{r}} u \ln\left(\dfrac{h_{\text{rg}}}{h} \right) \\[4mm]
C_{\text{p}} &= 1.9327 \times 10^{-10} T^4 - 7.999 \times 10^{-7} T^3 + 1.1407 \times 10^{-3} T^2 \\[2mm]
&\quad - 4.4890 \times 10^{-1} T + 1.0575 \times 10^3
\end{cases}
\tag{22}
$$

where k_{r} is the Von Karman constant and h_{rg} is the roughness length. The average PE matrix element $\overline{h_p^{pq}}$ and its dependence with temperature T, wind velocity u and antenna height h have been established through all the above equations. The following section presents results related to our purposes.

3. Results and discussion

This section shows how wind velocity and temperature influence PE gain; and what happens when we change antennas height and the distance between the transmitter and the receiver.

3.1. Wind speed and temperature effects on PE with $L = 80$ m and $h = 35$ m

Figure 3 shows coupled effects of wind speed and temperature when the distance between the transmitter and the receiver is 80 m and for antennas height of 35 m. This
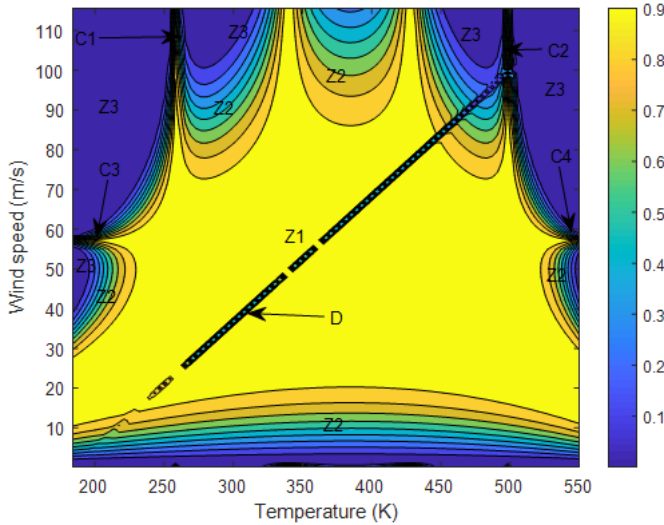
Fig. 3. Coupled effects of wind speed and temperature on PE with $L = 80$ m and $h = 35$ m.

figure presents an axial symmetry passing through the temperature of 375 K. Three principal zones are highlighted, and each zone is characterized by its average PE gain and delimitations through temperature and wind speed axis.

In the following, abbreviations Zi (Z for the abbreviation of zone; the index i corresponds to a specific zone represented in Fig. 3) and Zi(T, U, PE), (for a specific point of zone i; T, U, PE for temperature, velocity and PE components, respectively) are going to be used.

The highest average PE gain about [0.8 – 0.9] is observed in Z1 zone, and the lowest at zone Z3 is about [0.0 – 0.1]. Zone Z2 with PE factor between 0.12 and 0.79 is intermediate. One general observation is a nonlinear distribution of PE coefficients according to temperature and wind speed. When considering a fixed temperature of 375 K and following the vertical symmetry line (increased wind speed) in Fig. 3, we successively pass-through zone Z3 (characterized by lowest PE gain), Z2 (characterized by intermediate PE gain), Z1 (characterized by highest PE gain) then through Z2 (characterized by intermediate PE gain). The above data show that for a region with high temperature (375 K) and low wind velocity (0.1 m/s); if the wind of that region increases naturally or artificially from 0.1 to 9 m/s, it is going to increase PE gain from about 0.1 to 0.65. If that wind velocity still continues to increase from 9 to 30 m/s it is going to increase PE gain from about 0.75 to 0.9. However, if that wind velocity still continues to increase until it reaches 100 m/s, it is going to reduce PE gain until its lowest value. The distribution of PE gain according to temperature and wind speed represented in Fig. 3 also reveals four horns (C1, C2, C3, C4) characteristic of zones where PE gain tends to zero; and a mixed broken line (line D) is passing through Z1.

Misalignment or PE can occur due to a variety of reasons, such as swinging buildings, earthquakes, and heavy wind [43]. However, we generally omitted to add laser

beam wander phenomena as another potential cause of PE [44] during atmospheric turbulence. The beam wander which induced PE occurs when the size of eddies is larger than the optical beam size as shown in Fig. 1. In fact, atmospheric turbulence can be seen as combined effects of thermal turbulence due to thermal instability, characterized by Rayleigh number and dynamic turbulence due to wind speed instability character- ized by Reynolds number or by average turbulent kinetic energy per unit mass. That coupled effect of temperature and wind speed on PE can be explained by the fact that, for wind speed range of 0.1 to 9 m/s, at 375 K, the amount of turbulence large cells increases and causes the bend of laser beam. When wind speed increases from 9 to 30 m/s, PE gain increases from about 0.75 to 0.9, what can be explained by the fact that wind speed has the effect of dissipating thermal instability due to high temperature. However, over 100 m/s, PE gain is reduced until its lowest value due to the fact that Reynolds number reaches a critical value from which dynamic turbulence arises, so it appears to be a combined effects of thermal and dynamic turbulence which decrease PE gain.

Now, when considering the fixed wind speed of 50 m/s, and the increase in tem- perature, we observe that temperature can also reduce or increase the effect of dynamic turbulence concerning the amount of turbulence large cells which cause laser beam bend or PE. It is decreasing PE for some ranges of temperature and increasing PE for other temperature ranges. We observe that for low temperature (from 125 to 150 K) under wind speed of 50 m/s, we are in zone Z3 (lowest PE gain). When increasing tem- perature from 150 to 225 K, we inter to the zone Z2 (characterized by intermediate PE gain). For temperature range of 225 to 525 K under wind speed of 50 m/s, we are in zone Z1 (characterized by highest PE gain). However due to symmetrical behavior of PE distribution, we fall again in zone Z2 when we go beyond 525 K. That behavior can be explained by Rayleigh number which is characteristic of thermal instability or stability. In fact, 125 K could correspond to a frozen and icy atmosphere, it can also correspond to snow rain. Knowing that snow has a given refractive index, the natural or artificial increase in temperature will cause the snow to melt into water and then into steam. These different passages of atmospheric state, from the solid to vapor, will induce variation of the number of large size eddies through the variation of the refrac- tive-index structure. The above facts could explain these PE gain variations.

3.2. Wind speed and temperature effects on PE with L = 80 m and h = 30 m

When changing antennas height from 35 to 30 m, and letting unchanged the distance be- tween the transmitter and the receiver, the general shape of PE distribution according to wind speed and temperature remain unchanged as showed in Fig. 4. The symmetry, the three zones and four horns are still observed. However, we observed the reduction of the area of zone Z1 (characterized by highest PE gain) in the profit of zones Z2 (characterized by intermediate PE gain) and Z3 (characterized by lowest PE gain). In addition, we ob- served that the broken line D becomes a solid line. More specifically, the point zone Z1(325 K, 100 m/s, 0.85) for antennas height of 35 m becomes Z3(325 K, 100 m/s, 0.02)
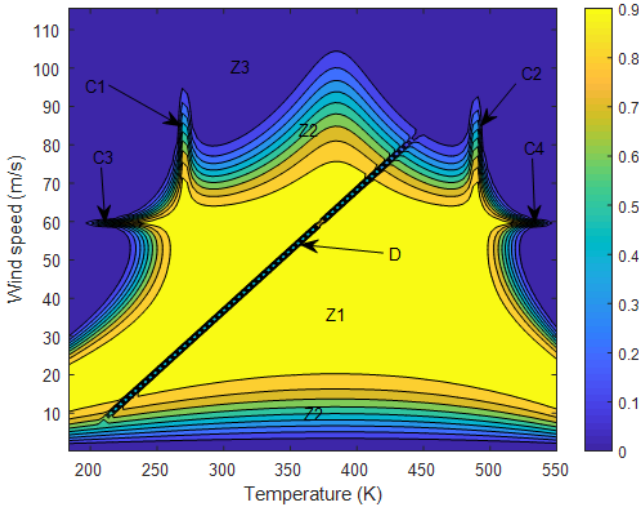
Fig. 4. Coupled effects of wind speed and temperature on PE with $L = 80$ m and $h = 30$ m.

when antennas height decreased from 35 to 30 m. That is to say, when we reduced antennas height by 5 m, the PE gain decreased from 0.85 to 0.02.

In fact, as soon as a fluid is fast transported on a roughly surface, it exchanges heat and the amount of movement nonlinearly by eddies. On the other hand, according to Taylor's hypothesis, experimentally demonstrated by [45, 46], the turbulence could be "frozen"; that is, the deformation of the vortices (eddies) due to the fluctuations is small compared to the advection due to the average velocity. So, under Taylor's frozen turbulence hypothesis, an eddy travels with the mean wind speed, while its size and characteristic parameters remain constant as shown in Fig. 2. Regarding the point zone Z1(325 K,100 m/s, 0.85) for antennas height of 35 m, by reducing antennas height from 35 to 30 m, the line-of-sight (LOS) between the emitter and the receiver directly enter in the "frozen eddies" which bend laser beam. As a result, we observed the decrease of PE gain from 0.85 to 0.02. The same explanation could be used for other points zones which have the same behavior.

3.3. Wind speed and temperature effects on PE with $L = 85$ m and $h = 30$ m

When changing the distance between the transmitter and receiver from 80 to 85 m, and letting the unchanged antennas height unchanged, the general shape of PE behavior according to wind speed and temperature is slightly changed as shown in Fig. 5. The symmetry is broken, and rather than of four horns, we now observe two. The three principal zones are still observed. However, we observed the reduction of the area of zone Z1 (characterized by highest PE gain which is between 0.8 and 0.9) in the profit of zones Z2 (characterized by intermediate PE gain which is between 0.12 and 0.79) and Z3 (characterized by lowest PE gain which is between 0.0 and 0.1). But the zone Z3 area is the most dominant. In addition, we observed that the broken line D becomes
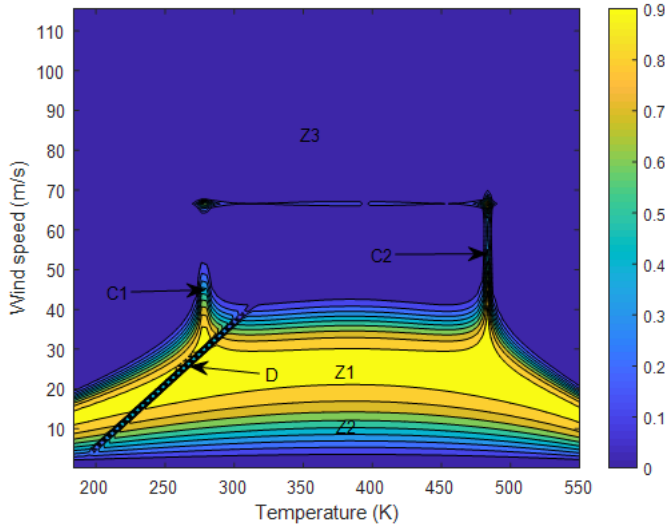
Fig. 5. Coupled effects of wind speed and temperature on PE with $L = 85$ m and $h = 30$ m.

a solid line and is translated towards regions of low temperatures. More specifically, the point zone Z1(375 K, 40 m/s, 0.85) for distance between the transmitter and the receiver of 80 m becomes Z3(375 K, 40 m/s, 0.02) when the distance between the transmitter and the receiver increased from 80 to 85 m. That is to say, when we increased the distance between the transmitter and the receiver by 5 m, the PE gain decreased from 0.85 to 0.02.

Those decreases of PE gain could be due to the "frozen eddies". In fact, when we modified the distance between the transmitter and the receiver from 80 to 85 m we introduced the "frozen eddies" in the LOS of antennas.

Generally, to establish an FSO link, technicians look for high rise buildings with direct visibility to install antennas there. The presence of frozen eddies in the direct visibility space will induce a decrease of PE gain. This is why our study suggests the installation of antennas with variable height (variable in all directions of space) and variable distance between the transmitter and receiver to get the link out of the frozen eddies zone as far as possible, in order to increase the PE gain.

4. Conclusion

The aims of this work were to study the coupled effects of temperature and wind speed on PE using matrix Rician pointing error (MRPE) model; then, to propose a new approach to reduce PE during FSO transmission in a turbulent environment. To achieve those purposes, average PE expression was established using MRPE. Then considering a Gaussian beam wave and Monin–Obukhov similarity functions for the structure parameters of temperature, explicit relationship was established between average PE, temperature and wind speed. It comes out of this study that there are nonlinear effects

of temperature and wind speed on PE. Under thermal turbulence, one can appropriately modify wind speed to reduced PE due to thermal instability. Reciprocally, under dynamic turbulence, one can appropriately modify temperature to reduced PE due to dynamic instability. Under specific atmospheric turbulence, an appropriate antenna height and the distance between transmitter and receiver choice led to reduced PE. Concerning turbulence strength which can be evaluated by the Rytov variance, our solution would be more efficient in case of weak and moderate large-scale turbulence. However, strong large-scale turbulence could be more difficult to handle.

References

[1] 10 Gbit/s Artolink Model [Online]. Available: http://artolink.com/ page/products/free space optics Artolink 10Gbps/ (2016).

[2] Saad W., Bennis M., Chen M., *A vision of 6G wireless systems: Applications, trends, technologies, and open research problems*, arXiv:1902.10265. https://doi.org/10.48550/arXiv.1902.10265

[3] Strinati E.C., Barbarossa S., Gonzalez-Jimenez J.L., Kténas D., Cassiau N., Dehos C., *6G: The next frontier*, arXiv:1901.03239. https://doi.org/10.48550/arXiv.1901.03239

[4] Soszka M., *Fading channel prediction for 5G and 6G mobile communication systems*, International Journal of Electronics and Telecommunications **68**(1), 2022: 153-160. https://doi.org/10.24425/ijet.2022.139863

[5] Yaacoub E., Alouini M.S., *A key 6G challenge and opportunity – connecting the remaining 4 billions: A survey on rural connectivity*, arXiv:1906.11541. https://doi.org/10.48550/arXiv.1906.11541

[6] Sibana K., Muyingi H.N., Mabanza N., *Building wireless community networks with 802.16 standard*, 3rd International Conference on Broadband Communications, Information Technology and Biomedical Applications, Gauteng, South Africa, November 2008.

[7] Alzenad M., Shakir M.Z., Yanikomeroglu H., Alouini M.S., *FSO-based vertical backhaul/fronthaul framework for 5G+ wireless networks*, IEEE Communications Magazine **56**(1), 2018: 218-224. https://doi.org/10.1109/MCOM.2017.1600735

[8] Laser Optronics Site [Online]. Available: http://www.laseropronics.com (2012).

[9] Al Naboulsi M., *Contribution à l'étude des liaisons optiques atmosphériques, propagation, disponibilité et fiabilité*, Thèse de doctorat, Université de Bourgogne, 2005.

[10] Andrews L.C., Phillips R.L., Hopen C.Y., Laser Beam Scintillation with Applications. Washington: SPIE Press, 2001.

[11] Alkholidi A.G., Altowij K.S., *Free space optical communications — Theory and practices*, [In] *Contemporary Issues in Wireless Communications*, [Ed.] M. Khatib, InTech, 2014. https://doi.org/10.5772/58884

[12] Arany L., Bhattacharya S., Macdonald J., Hogan S.J., *Simplified critical mudline bending moment spectra of offshore wind turbine support structures*, Wind Energy **18**(12), 2015: 2171-2197. https://doi.org/10.1002/we.1812

[13] Liu C., Yao Y., Sun Y., Zhao X., *Analysis of average capacity for free-space optical links with pointing errors over gamma-gamma turbulence channels*, Chinese Optics Letters **8**(6), 2010: 537-540.

[14] Borah D.K., Voelz D.G., *Pointing error effects on free-space optical communication links in the presence of atmospheric turbulence*, Journal of Lightwave Technology **27**(18), 2009: 3965-3973. https://doi.org/10.1109/JLT.2009.2022771

[15] GAO F., O'DONOGHUE T., WANG W., *Full-field analysis of wavefront errors in point diffraction interferometer with misaligned Gaussian incidence*, Applied Optics **59**(1), 2020: 210-216. https://doi.org/10.1364/AO.59.000210

[16] XU C., HAN W., WANG D., HUANG D., YUAN P., *Modeling and correction for the optical axis pointing error of an airborne electro-optical platform*, Applied Optics **58**(23), 2019: 6455-6463. https://doi.org/10.1364/AO.58.006455

[17] GAPPMAIR W., NISTAZAKIS H.E., *Subcarrier PSK performance in terrestrial FSO links impaired by gamma-gamma fading, pointing errors, and phase noise*, Journal of Lightwave Technology **35**(9), 2017: 1624-1632. https://doi.org/10.1109/JLT.2017.2685678

[18] HASSAN Z., HOSSAIN J., CHENG J., LEUNG V.C.M., *Effective capacity of coherent POLMUX OWC impaired by atmospheric turbulence and pointing errors*, Journal of Lightwave Technology **34**(21), 2016: 5007-5022. https://doi.org/10.1109/JLT.2016.2604345

[19] BOLUDA-RUIZ R., GARCÍA-ZAMBRANA A., CASTILLO-VÁZQUEZ C., CASTILLO-VÁZQUEZ B., HRANILOVIC S., *Amplify-and-forward strategy using MRC reception over FSO channels with pointing errors*, Journal of Optical Communications and Networking **10**(5), 2018: 545-552. https://doi.org/10.1364/JOCN.10.000545

[20] WANG J., ZHOU Y., BAI R., WANG G., *Point-ahead angle and coalignment error measurement method for free-space optical communication systems*, Journal of Lightwave Technology **35**(18), 2017: 3886-3893. https://doi.org/10.1109/JLT.2017.2718578

[21] BOLUDA-RUIZ R., GARCÍA-ZAMBRANA A., CASTILLO-VÁZQUEZ C., CASTILLO-VÁZQUEZ B., HRANILOVIC S., *Outage performance of exponentiated Weibull FSO links under generalized pointing errors*, Journal of Lightwave Technology **35**(9), 2017: 1605-1613. https://doi.org/10.1109/JLT.2017.2658956

[22] ZHOU Y., LU Y., HEI M., LIU G., FAN D., *Pointing error analysis of Risley-prism-based beam steering system*, Applied Optics **53**(25), 2014: 5775-5783. https://doi.org/10.1364/AO.53.005775

[23] FARID A.A., HRANILOVIC S., *Outage capacity optimization for free-space optical links with pointing errors*, Journal of Lightwave Technology **25**(7), 2007: 1702-1710. https://doi.org/10.1109/JLT.2007.899174

[24] DING J., XIE X., TAN L., MA J., KANG D., *Dual-hop RF/FSO systems over κ-μ shadowed and Fisher -Snedecor F fading channels with non-zero boresight pointing errors*, Journal of Lightwave Technology **40**(3), 2022: 708-719. https://doi.org/10.1109/JLT.2021.3120767

[25] HAN L., LIU X., WANG Y., LI B., *Joint impact of channel estimation errors and pointing errors on FSO communication systems over F turbulence channel*, Journal of Lightwave Technology **40**(14), 2022: 4555-4561. https://doi.org/10.1109/JLT.2022.3167035

[26] BALAJI K.A., PRABU K., *Performance evaluation of FSO system using wavelength and time diversity over Malaga turbulence channel with pointing errors*, Optics Communications **410**, 2018: 643-651. https://doi.org/10.1016/j.optcom.2017.11.006

[27] ANSARI I.S., YILMAZ F., ALOUINI M.-S., *Performance analysis of free-space optical links over Malaga (M) turbulence channels with pointing errors*, IEEE Transactions on Wireless Communications **15**(1), 2016: 91-102. https://doi.org/10.1109/TWC.2015.2467386

[28] ALSHAER N., ISMAIL T., NASR M.E., *Generic evaluation of FSO system over Málaga turbulence channel with MPPM and non-zero-boresight pointing errors*, IET Communications **14**(18), 2020: 3294-3302. https://doi.org/10.1049/iet-com.2020.0296

[29] BEN ISSAID C., PARK K.H., ALOUINI M.S., *A generic simulation approach for the fast and accurate estimation of the outage probability of single hop and multihop FSO links subject to generalized pointing errors*, IEEE Transactions on Wireless Communications **16**(10), 2017: 6822-6837. https://doi.org/10.1109/TWC.2017.2731947

[30] SANDALIDIS H.G., CHATZIDIAMANTIS N.D., KARAGIANNIDIS G.K., *A tractable model for turbulence- and misalignment-induced fading in optical wireless systems*, IEEE Communications Letters **20**(9), 2016: 1904-1907. https://doi.org/10.1109/LCOMM.2016.2584612

[31] Li M., Guo Y., Wang X., Fu W., Zhang Y., Wang Y., *Researching pointing error effect on laser linewidth tolerance in space coherent optical communication systems*, Optics Express **30**(4), 2022: 5769-5787. https://doi.org/10.1364/OE.447408

[32] Yi X., Yao M., *Free-space communications over exponentiated Weibull turbulence channels with nonzero boresight pointing errors*, Optics Express **23**(3), 2015: 2904-2917. https://doi.org/10.1364/OE.23.002904

[33] Yang F., Cheng J., Tsiftsis T.A., *Free-space optical communication with nonzero boresight pointing errors*, IEEE Transactions on Communications **62**(2), 2014: 713-725. https://doi.org/10.1109/TCOMM.2014.010914.130249

[34] Alheadary W.G., *Free Space Optics for 5G Backhaul Networks and Beyond*, Thesis for the Degree of Doctor of Philosophy, King Abdullah University of Science and Technology, July 2018, p. 26.

[35] Beckmann P., *Statistical distribution of the amplitude and phase of a multiply scattered field*, Journal of Research of the National Bureau of Standards **66D**(3), 1962: 231-240.

[36] Simon M.K., Alouini M.S., *Digital Communication over Fading Channel*, 2nd Ed., Wiley, New York City, USA, 2005.

[37] Andrews L.C., Phillips R.L., *Laser Beam Propagation Through Random Media*, Bellingham, Washington, 1998.

[38] Alda J., *Laser and Gaussian beam propagation and transformation*, Encyclopedia of Optical Engineering, Marcel Dekker Inc., New York, 2003.

[39] Prokes A., *Modeling of atmospheric turbulence effet on terrestrial FSO link*, Radioengineering **18**(1), 2009: 42-47.

[40] Ghassemlooy Z., Popoola W., Rajbhandari S., *Optical wireless communications: system and channel modelling with MATLAB*, CRC Press, Boca Raton, FL, 2012.

[41] Li D., Bou-Zeid E., H.A.R. De Bruin H.A.R., *Monin–Obukhov similarity functions for the structure parameters of temperature and humidity*, Boundary-Layer Meteorology **145**, 2012: 45-67. https://doi.org/10.1007/s10546-011-9660-y

[42] Specific Heat of Air vs. Temperature. users.wpi.edu

[43] Kaushal H., Kumar V., Dutta A., Aennam H., Jain V.K., Kar S., Joseph J., *Experimental study on beam wander under varying atmospheric turbulence conditions*, IEEE Photonics Technology Letters **23**(22), 2011: 1691-1693. https://doi.org/10.1109/LPT.2011.2166113

[44] Schlipf D., Trabucchi D., Bischoff O., Hofsäss M., Mann J., Mikkelsen T., Rettenmeier A., Trujillo J., Kühn M., *Testing of Frozen Turbulence Hypothesis for Wind Turbine Applications with a Scanning LIDAR System*, In Detaled Program ISARS. http://www.isars2010.uvsq.fr/

[45] Geng C., He G., Wang Y., Xu C., Lozano-Durán A., Wallace J.M., *Taylor's hypothesis in turbulent channel flow considered using a transport equation analysis*, Physics of Fluids **27**(2), 2015: 025111. https://doi.org/10.1063/1.4908070

[46] He X., He G., Tong P., *Small-scale turbulent fluctuations beyond Taylor's frozen-flow hypothesis*, Physical Review E **81**(6), 2010: 065303(R). https://doi.org/10.1103/PhysRevE.81.065303